Journal of Chromatography A, 1217 (2010) 2123–2131

Contents lists available at ScienceDirect

Journal of Chromatography A

journal homepage: www.elsevier.com/locate/chroma

pH Transients in hydroxyapatite chromatography columns—Experimental evidence and phenomenological modeling

Theresa E. Bankston, Laura Dattolo, Giorgio Carta*

Department of Chemical Engineering, University of Virginia, 102 Engineers' Way, Charlottesville, VA 22904-4741, USA

ARTICLE INFO

Article history:
Received 2 November 2009
Received in revised form 25 January 2010
Accepted 2 February 2010
Available online 6 February 2010

Keywords:
Hydoxyapatite
pH Transitions
Modeling
Local equilibrium theory

ABSTRACT

Hydroxyapatite (HAP) columns, widely used for chromatographic separation of proteins and other biomolecules because of their unique selectivity and ability to resolve complex mixtures, exhibit limited stability at acidic conditions requiring careful control of pH. Even with buffered solutions, however, unintended pH transients can occur when the salt concentration varies. For example, the pH temporarily decreases below the feed value when the salt concentration increases and increases above the feed value when the salt concentration is decreased. The intensity and duration of these transients depend on the particular buffer used and the magnitude of the salt concentration step, but in extreme cases the pH can drop by as much as 1.5 pH units creating conditions where the HAP stability is potentially compromised. This work examines the mechanisms leading to pH transients in HAP columns generated by salt steps. The pH excursions are similar to those observed for weak cation exchange columns, but are accompanied by a transient evolution of phosphate which temporarily decreases below the feed value when the salt concentration is increased and increases sharply when the salt concentration is reduced before returning to the feed value. A phenomenological model is developed to describe this behavior by considering the reversible uptake of sodium ions by the P-sites and binding of phosphate ions by the C-sites. The interplay of these two adsorption mechanisms results in complex pH patterns that are consistent with those observed experimentally. In addition to helping understand the underlying mechanisms, the model also provides a useful tool to predict the effects of different buffers and salt concentration and develop corrective measures that can reduce the intensity and duration of the pH transients such as the addition of unretained co-buffers.

1. Introduction

Hydroxyapatite (HAP), originally introduced by Tiselius et al. [1] is used extensively in both analytical and process scale chromatography separations of proteins and other biomolecules The friable and irregular HAP introduced early on has since been replaced by sintered ceramic hydroxyapatite forms, which are spherical in shape and much stronger mechanically [2] and many industrial applications have been developed [3–9]. The advantages of HAP rest primarily with its unique selectivity, which has been attributed to its multimodal functionality [10,11]. HAP is known to contain multiple adsorption sites: the so-called P-sites that are negatively charged and the so-called C-sites that are positively charged [9–14]. Accordingly, basic proteins in their cationic form are adsorbed mainly on the P-sites primarily as a result of electrostatic interactions. These proteins can be eluted with salts like NaCl in a step-wise or gradient fashion. Acidic proteins, on the other hand, are adsorbed mainly on the C-sites. These sites are thought to be positively charged calcium on the surface of the HAP crystals complexed with mobile phase phosphate. As suggested by the early work of Gorbunoff [10–12] as well as by recent studies by Schubert and Freitag [15] and Gagnon et al. [16] protein binding on these sites occurs primarily through the formation of coordination complexes between clusters of carboxyl groups or phosphate groups on the protein surface. Desorption of these proteins often requires competitive eluents, such as phosphate or citrate, which themselves form complexes with calcium. Of course, care must be taken in the practical use of strong complexing agents as eluents since dissolution of the HAP backbone can also occur. Surface-bound hydroxyl ions also exist. Although their role in protein adsorption is less clear, there have been suggestions that they could make a positive contribution to protein binding via hydrogen bonds [12]. The combination of P-site electrostatic interactions, C-site coordination, and, potentially, hydroxyl hydrogen bonding often affords very selective separations of complex mixtures. More practical considerations on the role of mobile phase modifiers can be found in Ref. [17].

A limitation of HAP is its modest stability at acidic conditions. The solubility product for neat HAP with stoichiometry

* Corresponding author. Tel.: +1 434 924 6281; fax: +1 434 982 2658.
E-mail address: gc@virginia.edu (G. Carta).

0021-9673/$ – see front matter © 2010 Elsevier B.V. All rights reserved.
doi:10.1016/j.chroma.2010.02.004

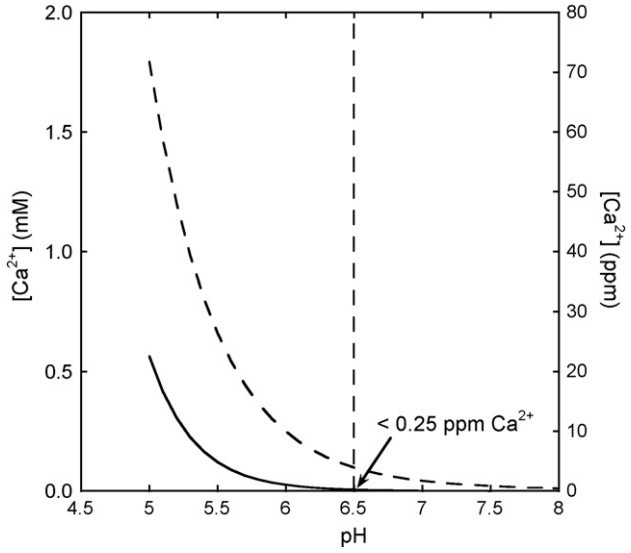

Fig. 1. Solubility of HAP in buffers containing no phosphate (dashed lines) and in buffers prepared with 5 mM Na_2HPO_4.

$Ca_5(PO_4)_3OH$ is defined by the following equation [18]:

$$K_s = [Ca^{2+}]^5[PO_4^{3-}]^3[OH^-] \quad (1)$$

where the terms in brackets represent thermodynamic activities. Empirical determinations of K_s are complicated by adsorbed species, which are released during the measurements causing substantial error, so that the span of the reported K_s-values is quite large [18]. Nonetheless, most modern measurements indicate values around 10^{-59} M^9 [19]. A value of $K_s = (2.03 \pm 0.71) \times 10^{-59}$ M^9 has been reported for NIST's HAP Standard Reference Material 2910 [20]. The solubility of HAP calculated with this value and expressed in terms of calcium concentration (on mM and ppm scales) is shown in Fig. 1 as an example. The calculations were done estimating activity coefficients from the extended Debye–Hückel Davies equation [21] both for buffers containing no phosphate and for buffers prepared using 5 mM Na_2HPO_4. As seen from these results, solubility decreases dramatically with the addition of phosphate because of the common ion effect, but increases rapidly even when 5 mM phosphate is added when the pH drops below 6.5. It should be noted that, in practice, the dissolution of HAP is also affected by kinetic factors, which, in turn, can be strongly influenced by thermal treatment or the addition of surface stabilizers to the HAP particles. However, even though the thermodynamic solubility predictions are worst-case scenarios and the actual stability is probably very dependent on the particular type of HAP used, it is obvious that operation below pH 6.5 can be problematic for extended use and that precise pH control is desirable during the typically used steps of load, wash, elution, strip, and regeneration. Unfortunately, this is not always easy to achieve. High amounts of phosphate in solution can affect retention of both basic and acidic proteins so that the mobile phase frequently has relatively low buffering capacity. An additional complication is that, in practice, even though the feed is buffered, significant pH excursions can occur in response to step or linear gradient changes in salt concentration. Recently, Cummings [22] has described pH drops as large as one pH unit for HAP columns operated with 5–10 mM phosphate buffers subject to 1 M NaCl steps. In each case, the pH drop was temporary but long lasting, requiring several column volumes to return to the feed value. Obviously, such transitions are a concern not only because of their potential effects on column stability but also because they can affect the retention behavior and stability of the eluted proteins.

The objective of this work is thus twofold. The first is to understand the mechanisms leading to pH transitions in HAP columns subject to step changes in feed composition. The second is to advance a phenomenological model for a semi-quantitative prediction of these effects useful as a tool to suggest ways in which the magnitude and duration of such pH transitions can be alleviated. For simplicity, our work is done without any applied protein sample, since, in practice, we expect that the general features would be the same except for extremely concentrated protein solutions.

2. Experimental

The hydroxyapatite used in this work was CHT® Ceramic Hydroxyapatite Type I obtained from Bio-Rad Laboratory (Hercules, CA, USA) with a 0.54 g/cm^3 nominal density, 60–80 nm pore size, and 40 ± 4 μm particle diameter. Samples of this material were packed in 10 mm × 100 mm Tricorn glass chromatography columns from GE Healthcare (Piscataway, NJ, USA) to a packed bed height of 11 cm using the procedure recommended by Bio-Rad. The column void volume was determined from the chromatographic retention of glucose, which gave a total column porosity $\varepsilon = 0.8$. The experiments were conducted with an AKTA Explorer 10 chromatographic workstation from GE Healthcare.

The buffer solutions used in this work were prepared as follows. Phosphate buffers were prepared by dissolving preset amounts of Na_2HPO_4 and NaCl in water and then adjusting the pH to 6.5 with the addition of concentrated phosphoric acid. MES buffers were prepared by adding MES acid to solutions containing preset amounts of NaOH and NaCl to attain a pH of 6.5. Thus, in each case, the sodium concentration is known precisely, while the concentration of the buffer species is varied to achieve the desired pH. For each experiment, the column was first equilibrated with approximately 20 column volumes of the initial buffer and then subject to step changes from low to high salt and vice versa. All column experiments were conducted at a flow rate of 4 cm^3/min, corresponding to a superficial velocity of 300 cm/h with a residence time of 2 min. The effluent conductivity was determined on line using the AKTA system monitor, while chloride, phosphate, and MES concentrations were determined by collecting 4 cm^3 (~0.5 CV) fractions and performing HPLC analyses. The pH was also determined off line for these fractions using a pH meter with a calibrated combination probe. HPLC analyses of chloride and phosphate were conducted with a Waters HPLC system (Milford, MA, USA) and a 4.1 mm × 150 mm PRP-X100 anion exchange column from Hamilton, Co. (Reno, NV, USA) with a mobile phase containing 4 mM p-hydroxybenzoic acid and 2.5% methanol adjusted to pH 8.5 with NaOH using non-suppressed conductivity detection with a Waters Model 430 detector. The flow rate was 2.0 cm^3/min and the injected sample volume was 20 μL.

3. Experimental results

Fig. 2 shows the pH transitions observed for four different cases, each with buffers at pH 6.5: 1000 mM positive and negative NaCl steps with a 5 mM Na_2HPO_4 buffer (Fig. 2a); 1000 mM positive and negative NaCl steps with a 10 mM NaMES buffer (Fig. 2b); positive and negative steps from 5 mM Na_2HPO_4 buffer to 50 mM Na_2HPO_4 (Fig. 2c); positive and negative steps from 10 mM NaMES to 5 mM Na_2HPO_4 buffer (Fig. 2d). As seen in these figures, negative and positive pH transients occur in all four cases. The pH drop and rise are greatest for the NaCl steps with phosphate buffer but decrease substantially in both intensity and duration when MES is used in lieu of phosphate. MES is zwitterionic and has a high buffering at pH 6.5, which leads to much better control of pH [23,24]. Unfortunately, however, operation without phosphate is unfeasible for prolonged

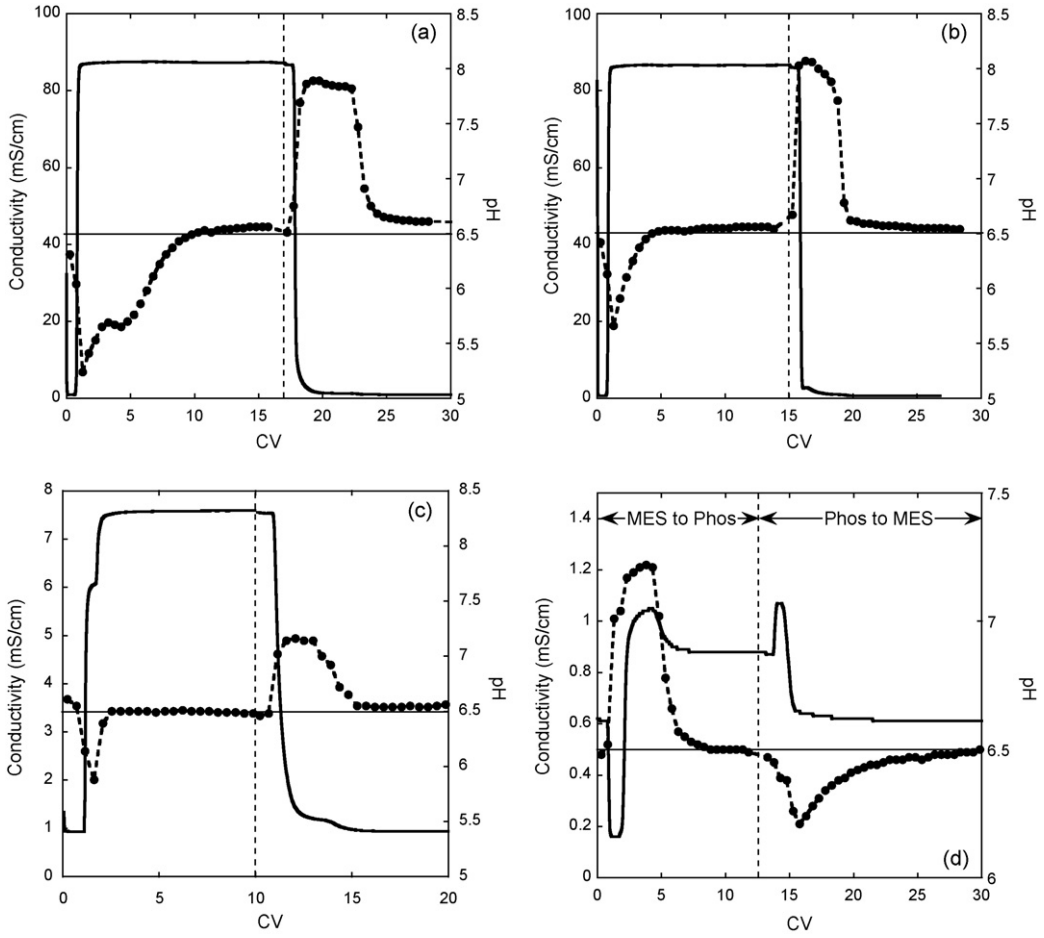

Fig. 2. pH (dots) and conductivity (solid lines) transitions obtained with a CHT® Type I column with buffers at pH 6.5. (a) 1000 mM positive and negative NaCl steps with a 5 mM Na_2HPO_4 buffer; (b) 1000 mM positive and negative NaCl steps with a 10 mM NaMES buffer; (c) positive and negative steps from 5 mM Na_2HPO_4 buffer to 50 mM Na_2HPO_4; (d) positive and negative steps from 10 mM NaMES to 5 mM Na_2HPO_4 buffer.

times, since the HAP will eventually dissolve as suggested by Fig. 1. As seen in Fig. 2c, pH transitions occur also in the absence of chloride when the sodium and phosphate concentrations are changed. Interestingly, as seen in Fig. 2d, they also occur, albeit to smaller extent, even when the sodium concentration is kept constant but the buffer is changed from MES to phosphate and vice versa.

pH transients have also been observed for ion exchange chromatography columns containing weak acid groups in response to NaCl steps using unretained buffers [24–26]. In this case, the pH transitions result from the reversible uptake of sodium ions by the stationary phase in exchange for protons, which are released into the flowing liquid. As a result, the pH decreases below the feed value in response to positive salt steps and increases in response to negative steps. In this respect, these pH transitions are similar to the ones observed for HAP columns. However, the latter are obviously more complex when phosphate is present. In this case, three different waves appear to travel through the column in response to a salt step. The fastest of these waves emerges in about 1 CV and likely corresponds to the passage of unretained species. The other two waves elute later and are likely related to the exchange of adsorbed species between the stationary phase and the mobile phase.

In order to understand this behavior, experiments were done by measuring the concentration of phosphate and chloride in addition to pH. The results are shown in Figs. 3–5 for different NaCl steps. It can be seen that while chloride appears to be indifferent to the HAP surface and passes through in about 1 CV, the phosphate concentration drops to a low level following the positive NaCl step before returning to the feed value and increases dramatically above the feed value following the negative NaCl step. Corresponding transitions are seen for the conductivity traces, which closely mimic the Na^+ concentration. Intermediate plateaus are also seen for both phosphate and conductivity where values different from both the feed and initial solutions are attained. Note that reducing the magnitude of the NaCl step reduces the magnitude and duration of the pH transitions affecting the phosphate profile in a corresponding way but does not change the overall shape of the transitions.

4. Model development

The experimental evidence provided thus far suggests that a minimum of three species, including two absorbable ones, must be considered in order to predict the pH transitions in HAP columns. Two adsorbable plus a non-adsorbed species are expected to result in three waves traveling through the column when the NaCl concentration is stepped up or down as illustrated in Fig. 6. The fastest wave corresponds to the passage of unretained chloride ion, while the two slower waves are associated with the simultaneous adsorption of Na^+ and phosphate. Intermediate states are formed between the fast wave and the two slower waves. There is considerable evidence in the literature that reversible adsorption of Na^+ and phosphate occurs on the HAP surface. It is well established, for example, that HAP has a point of zero charge (PZC) around pH 7, where the electrophoretic mobility is zero [27,28]. This can be explained by the protonation of P-sites at low pH and their deprotonation at high pH. By mass action law, increasing Na^+ drives their

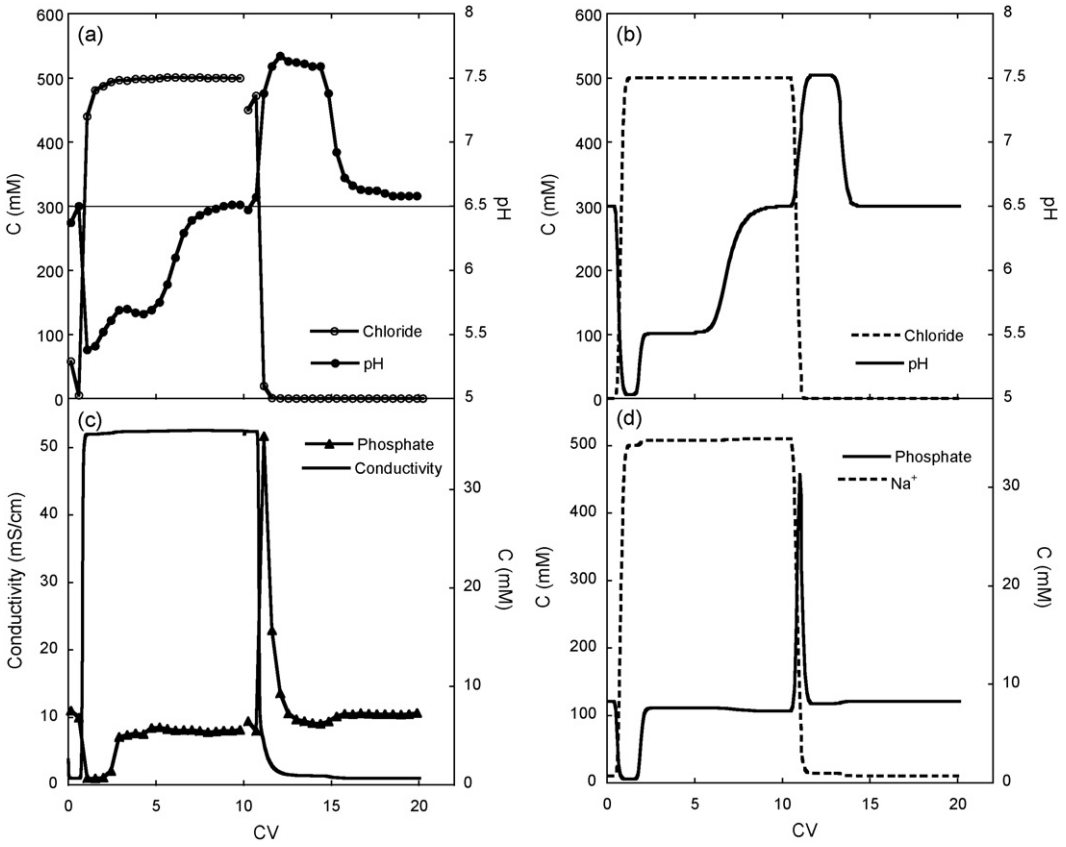

Fig. 3. Experimental (left) and simulated (right) transitions obtained with a CHT® Type I column for 500 mM positive and negative NaCl steps with a 5 mM Na_2HPO_4 buffer at pH 6.5. (a) and (b) Chloride and pH, (c) and (d) phosphate and conductivity (or Na^+).

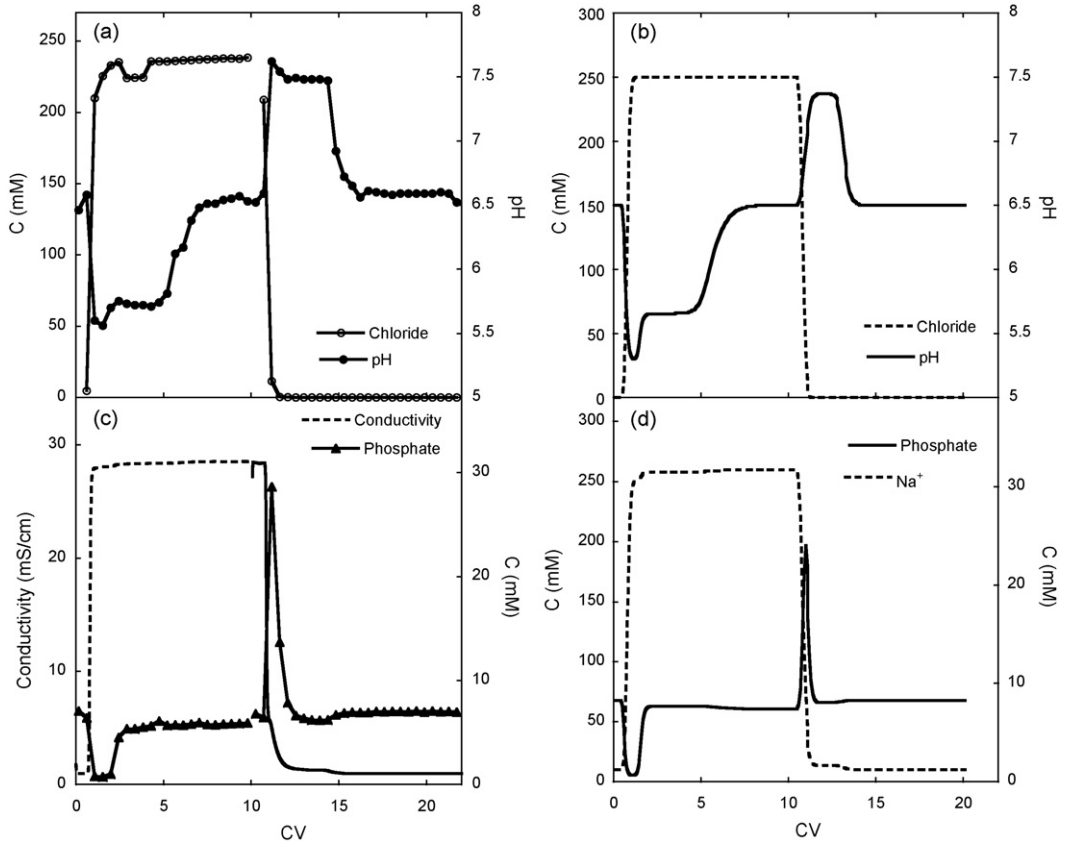

Fig. 4. Experimental (left) and simulated (right) transitions obtained with a CHT® Type I column for 250 mM positive and negative NaCl steps with a 5 mM Na_2HPO_4 buffer at pH 6.5. (a) and (b) Chloride and pH, and (c) and (d) phosphate and conductivity (or Na^+).

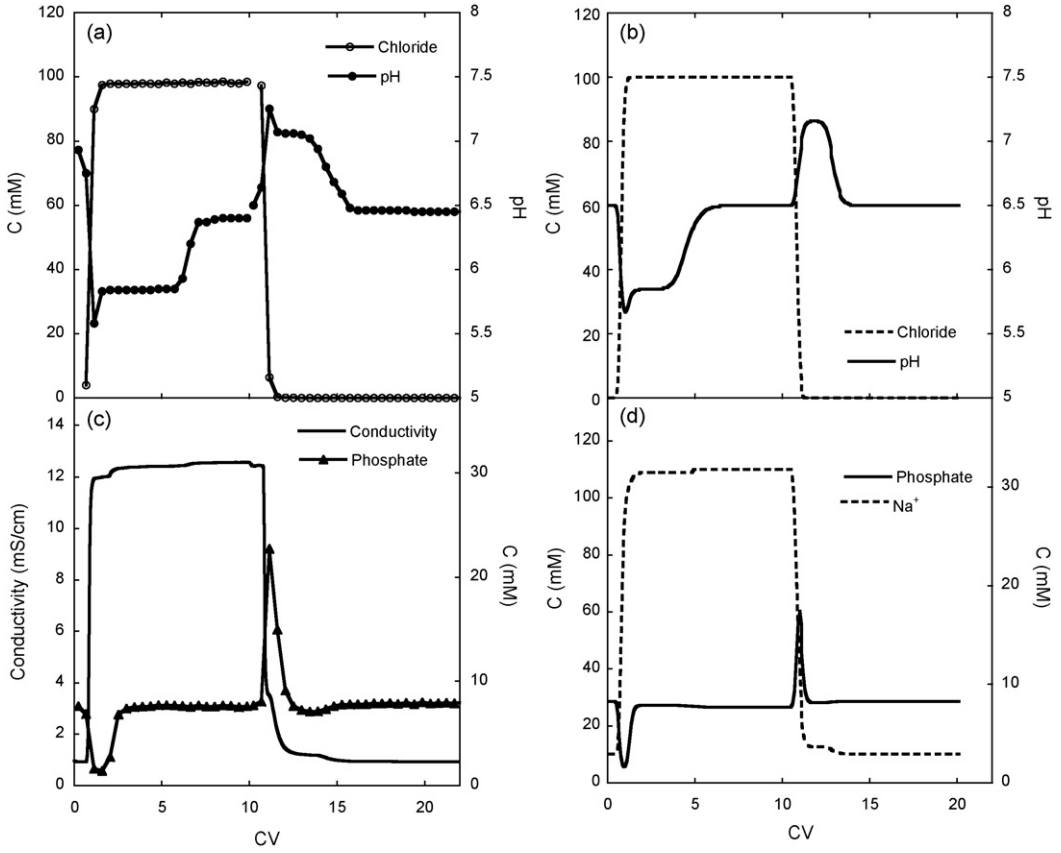

Fig. 5. Experimental (left) and simulated (right) transitions obtained with a CHT® Type I column for 100 mM positive and negative NaCl steps with a 5 mM Na_2HPO_4 buffer at pH 6.5. (a) and (b) Chloride and pH, and (c) and (d) phosphate and conductivity (or Na^+).

deprotonation resulting in a release of protons to the solution and "adsorption" of Na^+. The fact that the PZC occurs at pH values close to the $pK_{a,2}$ of phosphate in solution suggests that the P-sites are formed by surface exposed phosphate groups from the HAP crystals. More recent results by Harding et al. [29] confirm this behavior through surface titrations used to determine the Bronsted acidity of the surface. As shown by these authors, HAP removes protons from solution as the pH is lowered and releases them in exchange for Na^+ when the pH is increased.

There is also ample evidence in the literature suggesting that dissolved phosphate ions are readily adsorbed onto the surface of HAP. Hodge et al. [30], for example, measured phosphate adsorption onto HAP from Na_2HPO_4 solutions at 40 °C with phosphate concentrations ranging from 0.00002 to 0.2 M using radioactive P. These authors observed an isotherm behavior with maximum phosphorous uptake of 45.7 mg/g HAP. Doss [27] measured the electrophoretic mobility of HAP as a function of the addition of acids or bases. This author found that addition of H_3PO_4 lowered the pH of the HAP suspension but did not affect the electrophoretic mobility and explained this behavior by hypothesizing that hydrogen and phosphate ions are co-adsorbed on the HAP surface with equal affinity. Shimbayashi et al. [31] measured phosphate adsorption on HAP based on depletion of solutions of Na_2HPO_4 or K_2HPO_4 at pH values in the range 9.3–9.6. For these conditions, phosphate adsorption was characterized by a very favorable isotherm at low phosphate concentrations, with a Langmuir behavior and maximum capacity around 0.25 mmol/g HAP at higher concentrations. Shimbayashi et al. also investigated the effect of pH on phosphate adsorption by HAP. Reducing pH from 10 to 6 by the addition of HCl resulted in an increase of phosphate adsorption from about 0.2 to about 0.3 mmol/g HAP for Na_2HPO_4 solutions and from about 0.15 to about 0.27 mmol/g HAP for K_2HPO_4 solutions. In these experiments, phosphate adsorption was essentially independent of the K^+ concentration for K_2HPO_4 solutions and only weakly dependent on the Na^+ concentration for Na_2HPO_4 solutions. The effect of pH was attributed to lower mutual repulsion between adsorbed phosphate ions as the pH is reduced and the phosphate is protonated. Similar results have been reported more recently by Gasser at al. [28] at pH 6.85. Finally, adsorption of phosphate species on HAP has also been observed by NMR spectroscopy by Fukegawa et al. [32].

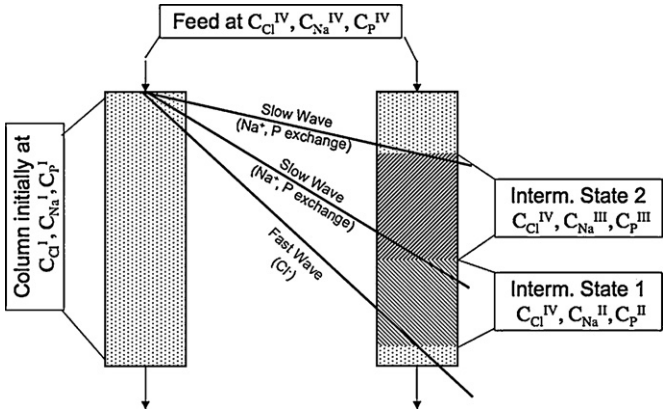

Fig. 6. Schematic of concentration waves generated in response to a salt concentration step. States *I* and *IV* are the initial and feed states. States *II* and *III* are intermediate states.

Since the goal of this work is to develop a phenomenological model, independent measurements of Na^+ and phosphate

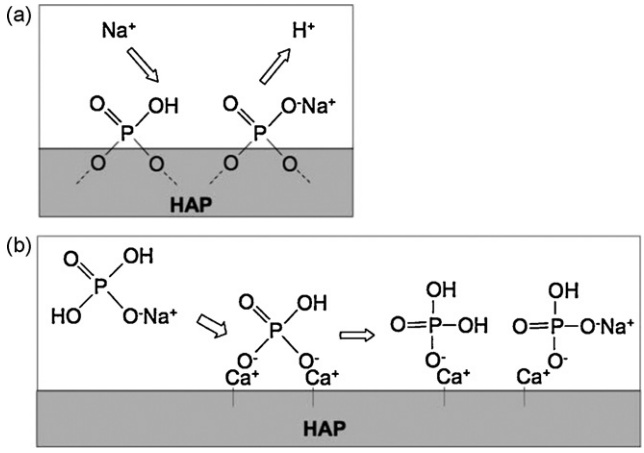

Fig. 7. Hypothesized mechanisms of Na^+ and phosphate binding to hydroxyapatite: (a) P-sites and (b) C-sites.

adsorption were not made. However, the literature information was used to create a suitable model as follows. We assume that P- and C-sites interact with Na^+ and phosphate independently as shown schematically in Fig. 7. For the P-sites we assume that deprotonation occurs according to the following equilibrium relationship:

$$PH = P^- + H^+, \quad K = \frac{q_{P^-} q_{H^+}}{q_{PH}} \tag{2}$$

where the q_i's represent surface-bound concentrations. A balance yields the following result:

$$q_P^0 = q_{PH} + q_{P^-} \sim q_{PH} + q_{Na^+} \tag{3}$$

where q_P^0 is the concentration of P-sites. The second equality in Eq. (3) is obtained by analogy to the case of weak cation exchangers [33] neglecting the concentration of free H^+ on the surface. This is reasonable as long as there is minimum degree of deprotonation and $C_{Na^+} \gg C_{H^+}$ which occurs provided the pH is not too low (e.g. pH > 3). Finally, based on Donnan equilibrium, we can relate the surface-bound proton and Na^+ concentrations to the corresponding values in solution through the following equation:

$$\frac{q_{Na^+}}{q_{H^+}} = \frac{C_{Na^+}}{C_{H^+}} \tag{4}$$

The latter can be obtained by equating the electrochemical potentials of surface-bound H^+ and Na^+ to the corresponding values in solution and eliminating the electrical potential difference between surface and bulk solution phases. The final result is obtained combining by Eqs. (2)–(4), which yields:

$$q_{Na^+} = \frac{1}{2}\left\{ -\frac{KC_{Na^+}}{C_{H^+}} + \left[\left(\frac{KC_{Na^+}}{C_{H^+}} \right)^2 + 4q_P^0 \frac{KC_{Na^+}}{C_{H^+}} \right]^{0.5} \right\} \tag{5}$$

This result is formally the same as that obtained for weak cation exchangers [24,33] and indicates that Na^+ adsorption is regulated by the ratio of Na^+ and H^+ concentrations in solution. We assume that the equilibrium constant is pK = 7.21 as for the dissociation of divalent phosphate in solution.

From the foregoing discussion, it is apparent that phosphate is adsorbed selectively. In fact, even in 1000 mM chloride, phosphate is adsorbed when the pH drops. Obviously, this cannot be the result of ordinary ion exchange, since the large excess of chloride would likely displace phosphate ions. Thus, we assume that binding of phosphate ions occurs through the site-sharing mechanism shown schematically in Fig. 7 and similar to that described by Helfferich [33] for adsorption of phosphoric acid by phosphate-form anion exchangers. When the pH drops as a result of Na^+ uptake by the P-sites, more phosphate is converted from divalent to monovalent form. Thus, additional phosphate is bound. On the other hand, when the pH rises following release of Na^+ from the HAP surface, more phosphate becomes divalent. For these conditions, a smaller amount of phosphate can be bound and the excess is desorbed. Quantitatively, we describe this process with the following exchange on the C-sites at the HAP surface:

$$Ca_2HPO_4 + H_2PO_4^- + Na^+ = CaH_2PO_4 + CaHPO_4Na \tag{6}$$

with equilibrium constant:

$$K_c = \frac{q_{H_2PO_4^-} q_{HPO_4^{2-}Na^+}}{q_{H_2PO_4^{2-}} C_{H_2PO_4^-} C_{Na^+}} \tag{7}$$

This expression is consistent with the observations of Shimabayashi et al. [31] who noted that phosphate binding on HAP is determined by the ionic product of phosphate and sodium ions. Combining Eq. (7) with the following C-site balance:

$$q_C^0 = q_{H_2PO_4^-} + 2q_{HPO_4^{2-}} \tag{8}$$

and assuming that $q_{H_2PO_4^-} = q_{HPO_4^{2-}Na^+}$, yields the result:

$$q_{H_2PO_4^-} = \frac{1}{2}\left\{ -\frac{K_c C_{H_2PO_4^-} C_{Na^+}}{2} + \left[\left(\frac{K_c C_{H_2PO_4^-} C_{Na^+}}{2} \right)^2 + 2q_C^0 K_c C_{H_2PO_4^-} C_{Na^+} \right]^{0.5} \right\} \tag{9}$$

$$q_{HPO_4^{2-}} = \frac{1}{2}(q_C^0 - q_{H_2PO_4^-}) \tag{10}$$

where q_C^0 is the concentration of C-sites. Finally, the total adsorbed phosphate is given by:

$$q_P = 2q_{H_2PO_4^-} + q_{HPO_4^{2-}} \tag{11}$$

Note that additional Na^+ is adsorbed along with phosphate per Eq. (6).

The final components of the model needed to predict the column dynamic behavior are material balances for chloride, Na^+, and total phosphate and the electroneutrality condition. Neglecting axial dispersion, the former are given by the following equations with time, t, and distance, z, as independent variables:

$$\varepsilon \frac{\partial C_{Cl^-}}{\partial t} + \varepsilon v \frac{\partial C_{Cl^-}}{\partial z} = 0 \tag{12}$$

$$\varepsilon \frac{\partial C_{Na^+}}{\partial t} + (1-\varepsilon)\frac{\partial q_{Na^+}}{\partial t} + \varepsilon v \frac{\partial C_{Na^+}}{\partial z} = 0 \tag{13}$$

$$\varepsilon \frac{\partial C_P}{\partial t} + (1-\varepsilon)\frac{\partial q_P}{\partial t} + \varepsilon v \frac{\partial C_P}{\partial z} = 0 \tag{14}$$

where ε is the column void fraction, v is the interstitial velocity, C_{Cl^-}, C_{Na^+}, and C_P are the total chloride, Na^+, and phosphate solution concentrations, and q_{Na^+} and q_P are the corresponding quantities adsorbed on the HAP surface. Note that $q_{Cl^-} = 0$ since, as shown by the experimental data, chloride is unretained and elutes in about 1 CV. Assuming local equilibrium, q_{Na^+} and q_P are related to the solution composition via Eqs. (5) and (9), respectively. The electroneutrality condition is given by

$$C_{Na^+} + C_{H^+} = 2C_{HPO_4^{2-}} + C_{H_2PO_4^-} + C_{Cl^-} + C_{OH^-} \tag{15}$$

or, considering the deprotonation constant of monovalent phosphate, $K'_{a,2}$, and the ionic product of water, K'_W:

$$C_{Na^+} + C_{H^+} = \frac{2K'_{a,2} + C_{H^+}}{K'_{a,2} + C_{H^+}} C_P + C_{Cl^-} + \frac{K'_W}{C_{H^+}} \tag{16}$$

Note that $K'_{a,2}$ and K'_W are corrected equilibrium constant accounting for solution ionic strength as discussed in Ref. [24]. For given values of C_{Cl^-}, C_{Na^+}, and C_P, Eq. (16) is only a function of C_{H^+} which can be solved for iteratively in order to find the solution $pH = -\log(\gamma_{H^+} C_{H^+})$.

5. Model solution and predictions

The model equations (Eqs. (5), (9), (12)–(14) and (16)) were solved in two different ways. A numerical solution was obtained by discretizing the axial derivatives by backward finite differences and integrating the resulting system of ordinary differential equations in time using subroutine DIVPAG of the IMSL library. Since the discretization introduces numerical dispersion, the number of discretization points can be used to describe deviations from ideality. In our case, however, this number was kept relatively high (40) in order to approximate ideal conditions. An analytical solution was obtained by the method of characteristics [24,33,34] assuming, for simplicity, that all of the transitions are either contact discontinuities or coherent shocks [34]. In this case, each component has characteristic velocity:

$$v_{s,i} = \frac{v}{1 + \phi(\Delta q_i / \Delta C_i)} \tag{17}$$

where $\phi = (1 - \varepsilon)/\varepsilon$. For each wave the characteristic velocities are equal for all components. With reference to Fig. 6, since there is no adsorption of chloride for the fast wave we have:

$$v_{s,Cl^-} = v_{s,Na^+} = v_{s,P} = v \tag{18}$$

or:

$$\Delta q_{Na^+} = \Delta q_P = 0 \tag{19}$$

where Δ indicates the difference between values upstream and downstream of the wave front. The composition downstream of this front is $C^I_{Cl^-}, C^I_{Na^+}, C^I_P$. Since chloride is not adsorbed, immediately upstream we have $C_{Cl^-} = C^{IV}_{Cl^-}$. Na^+ and phosphate concentrations can then be calculated based on Eq. (19) by solving the following system of equations:

$$q_{Na^+}(C^I_{Cl^-}, C^I_{Na^+}, C^I_P) = q_{Na^+}(C^{IV}_{Cl^-}, C^{II}_{Na^+}, C^{II}_P) \tag{20}$$

$$q_P(C^I_{Cl^-}, C^I_{Na^+}, C^I_P) = q_P(C^{IV}_{Cl^-}, C^{II}_{Na^+}, C^{II}_P) \tag{21}$$

where the functions q_{Na^+} and q_P are given by Eqs. (5), (9) and (16). The maximum H^+ concentration (or minimum pH) during a salt step up, is obtained when $C^{II}_P = 0$, which occurs if phosphate binding is infinitely favorable. In this case, Eqs. (5), (16) and (20) yield:

$$\frac{C^I_{Na^+}}{C^I_{H^+}} = \frac{C^{II}_{Na^+}}{C^{II}_{H^+}} \sim \frac{C^{IV}_{Cl^-}}{C^{II}_{H^+}} \tag{22}$$

Thus, for a 500 mM NaCl step with a 5 mM Na_2HPO_4 buffer at pH 6.5, as in Fig. 3, we have approximately $(C^{II}_{H^+})_{min} \sim C^{IV}_{Cl^-}(C^I_{H^+}/C^I_{Na^+}) \sim 0.5(10^{-6.5}/10^{-2}) = 1.58 \times 10^{-5}$ M, or a pH of approximately 4.8. In practice, the actual pH achieved with the fast wave is higher since $C^{II}_P \neq 0$ as a result of the fact that phosphate binding is not infinitely favorable. The actual value is calculated from Eqs. (20) and (21) and is shown in Fig. 8.

The composition of the intermediate states *II* and *III* formed between the two slow waves with a positive salt step are found by solving the following two equations derived by equating the wave velocities for Na^+ and phosphate:

$$\frac{q_{Na^+}(C^{IV}_{Cl^-}, C^{II}_{Na^+}, C^{II}_P) - q_{Na^+}(C^{IV}_{Cl^-}, C^{III}_{Na^+}, C^{III}_P)}{C^{II}_{Na^+} - C^{III}_{Na^+}} = \frac{q_P(C^{IV}_{Cl^-}, C^{II}_{Na^+}, C^{II}_P) - q_P(C^{IV}_{Cl^-}, C^{III}_{Na^+}, C^{III}_P)}{C^{II}_P - C^{III}_P} \tag{23}$$

$$\frac{q_{Na^+}(C^{IV}_{Cl^-}, C^{III}_{Na^+}, C^{III}_P) - q_{Na^+}(C^{IV}_{Cl^-}, C^{IV}_{Na^+}, C^{IV}_P)}{C^{III}_{Na^+} - C^{IV}_{Na^+}} = \frac{q_P(C^{IV}_{Cl^-}, C^{III}_{Na^+}, C^{III}_P) - q_P(C^{IV}_{Cl^-}, C^{IV}_{Na^+}, C^{IV}_P)}{C^{III}_P - C^{IV}_P} \tag{24}$$

The corresponding wave velocities and elution times are found from Eq. (17) and number of column volumes is calculated as $CV = \varepsilon v_s t/L$ where L is the column length. The same procedure provides the intermediate states *V* and *VI* attained during the salt step down shown in Fig. 8. As seen in this figure, it is clear that there is substantial agreement between analytical and numerical solutions, although, of course, smoother, constant-pattern transitions rather than shocks are obtained with the numerical solution.

For a quantitative comparison with the experimental results, the four model parameters K, q^0_p, K_c, and q^0_C must be determined. As previously noted, K was assumed to be the same as the dissociation constant of monovalent phosphoric acid in solution. Unfortunately, however, not enough information is available in the literature to determine the three remaining parameters, in part because the available data are not for the same apatite used in this work. Thus, q^0_p, K_c, and q^0_C were fitted to the experimental data with 500 mM NaCl steps and are summarized in Table 1. Model predictions obtained from the numerical solution using these parameters

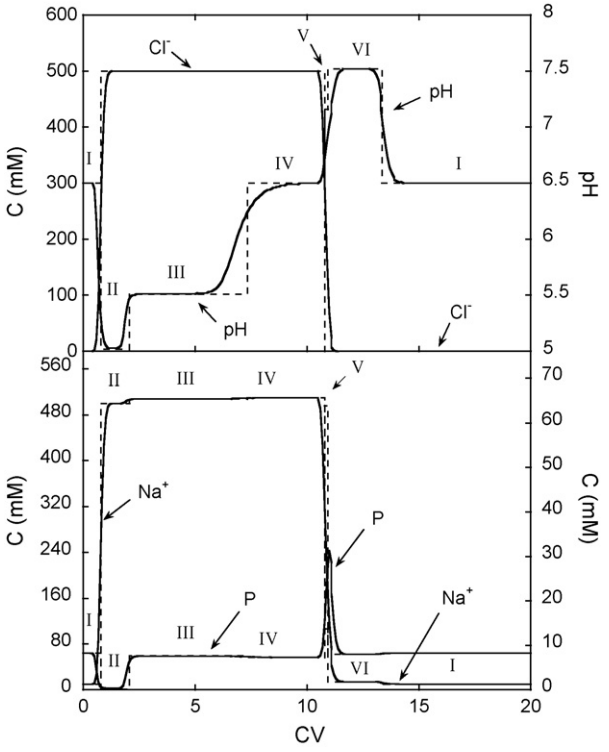

Fig. 8. Comparison of numerical solution (solid lines) and analytical solution (dashed lines) for a 500 mM NaCl step using the parameters in Table 1. Intermediate states are *II* and *III* for the salt step up and *V* and *VI* for the salt step down. Conditions simulated are as in Fig. 3.

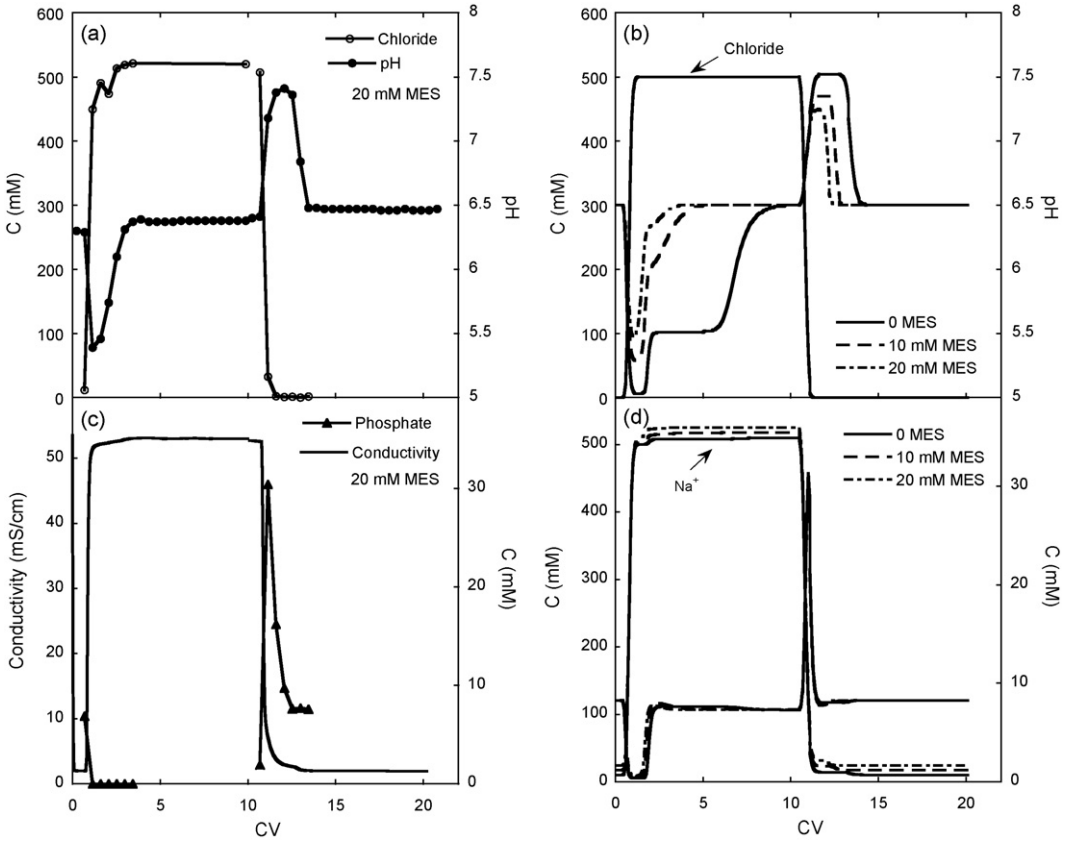

Fig. 9. Comparison of experimental (left) and predicted (right) transitions obtained with a CHT® Type I column for 500 mM positive and negative NaCl steps with a 5 mM Na_2HPO_4 buffer at pH 6.5 with the addition as MES as a co-buffer. (a) and (b) Chloride and pH and (c) and (d) phosphate and conductivity (or Na^+).

Table 1
Model parameters.

Parameter	Value	Units
ε	0.8	–
pK	7.21	M
q_P^0	300	μmol/mL solid
	60	μmol/mL column[a]
q_C^0	200	μmol/mL solid
	40	μmol/mL column[a]
K_c	5.0	M^{-1}

[a] Value calculated as $q \times (1-\varepsilon)$.

are shown in Figs. 3–5. The model predicts the correct wave shapes and is in semi-quantitative agreement.

It should be noted that we have neglected to account explicitly for any dissolution of HAP. However, based in Fig. 1, even assuming that the mobile phase becomes saturated, the phosphate concentration derived from dissolved HAP would be on the order of 0.5–1 mM, which is quite small compared to the actual phosphate concentration swings observed. This result indicates that the pH swings can be predicted with reasonable accuracy even though dissolution is neglected, providing a useful practical tool to investigate how such pH swings can be mitigated.

One approach to mitigate the pH transitions is to use unretained co-buffers such as MES as suggested empirically by Cummings [22]. MES is zwitterionic and is deprotonated to form a negatively charged sulfonate species, MES^-. Our model is easily modified to predict the pH excursions for this case by adding the additional material balance:

$$\varepsilon\frac{\partial C_{MES}}{\partial t} + \varepsilon v\frac{\partial C_{MES}}{\partial z} = 0 \tag{25}$$

and rewriting the electroneutrality condition as follows:

$$C_{Na^+} + C_{H^+} = 2C_{HPO_4^{2-}} + C_{H_2PO_4^-} + C_{MES^-} + C_{Cl^-} + C_{OH^-} \tag{26}$$

or:

$$C_{Na^+} + C_{H^+} = \frac{2K'_{a,2} + C_{H^+}}{K'_{a,2} + C_{H^+}}C_P + \frac{K'_{a,1}}{K'_{a,1} + C_{H^+}}C_{MES} + C_{Cl^-} + \frac{K'_W}{C_{H^+}} \tag{27}$$

where C_{MES} and C_{MES^-} are the concentrations of total and negatively charged MES and $K'_{a,1}$ is the activity-coefficient corrected dissociation constant of MES zwitterions. The latter has a value of p$K_{a,1}$ = 6.2 at infinite dilution [23]. Model prediction are shown in Fig. 9 for different MES concentrations using the parameters in Table 1 in comparison with experimental data obtained with 20 mM MES co-buffer concentration. The results confirm both the value of using co-buffers as well as the predictive ability of the model. Both magnitude and duration of the pH transitions are greatly reduced. Of course, the Na^+ concentration (and the ionic strength) is increased so that the NaCl concentration would likely have to be adjusted accordingly in order to obtain equivalent protein elution behavior. However, since MES is not retained significantly by HAP, protein adsorption is likely to be unaffected.

6. Conclusions

It is well established that HAP is a multifunctional material containing both negatively charged binding sites (the so-called P-sites) and positively charged binding sites (the so-called C-sites). This combination results in unique selectivity and affords the ability to separate complex mixtures. However, it also causes complex pH transients in response to changes in salt concentration and buffer composition at the column entrance. Our experimental results are

consistent with a mechanism where Na^+ is retained by the P-sites with concomitant release of protons into the mobile phase when the NaCl concentration is increased. In turn, the released protons associate with phosphate ions in solution, which become absorbed on the C-sites by a site-sharing mechanism. The opposite occurs when the NaCl concentration is decreased. In this case, the pH rises since Na^+ is desorbed, and surface-bound phosphate is released. The results show that chloride is not adsorbed by HAP and is not by itself responsible for the pH transitions, which occur even when only phosphate is present as long as the Na^+ and/or phosphate concentration changes. MES also appears to be unadsorbed and can be used as a co-buffer to mitigate the magnitude and duration of the pH transients. The phenomenological model developed in this work, while tentative, provides a good description of the observed phenomena yielding wave shapes that are consistent with the experiments. The model also has predictive value and can be used to assess the effects of co-buffers added to control the pH transients and, potentially, to explain the interaction of pH waves with the elution of bound proteins. A potentially important aspect not considered explicitly in this work is the effect of flow rate or residence time. In general higher flow rates and lower residence times can be expected to broaden the pH transitions. However, since the pH effects observed in this work are caused by the exchange of small ions, the effects of mass transfer resistances and, hence, residence time are expected to be relatively small. As a result, the pH profiles are fairly close to the local equilibrium limit as seen in Fig. 8 even at the relatively high flow rates used in this work.

Acknowledgements

This research was supported by Bio-Rad Laboratories, by Merck & Co., Inc., and by NSF Grant No. CTS-0729857.

References

[1] A. Tiselius, S. Hjerten, O. Levin, Arch. Biochem. Biophys. 65 (1956) 132.
[2] P. Ng, A. Cohen, V. McLaughlin, Bioprocess Int. 4 (2006) 46.
[3] R. Giovannini, R. Freitag, Bioseparation 9 (2000) 359.
[4] R. Giovannini, R. Freitag, Biotechnol. Bioeng. 77 (2002) 445.
[5] E. Dolinski, K. Hawkins, J. Myers, Process-scale ceramic hydroxyapatite chromatography: benefits and issues, Abstracts of Papers of the American Chemical Society, 224 (2002) 318-BIOT Part 1.
[6] A. Jungbauer, R. Hahn, K. Deinhofer, P. Luo, Biotechnol. Bioeng. 87 (2004) 364.
[7] S. Schubert, R. Freitag, J. Chromatogr. A 1142 (2007) 106.
[8] D.L. Wensel, B.D. Kelley, J.L. Coffinan, Biotechnol. Bioeng. 100 (2008) 839.
[9] P. Gagnon, New Biotechnol. 25 (2009) 287.
[10] M.J. Gorbunoff, Anal. Biochem. 136 (1984) 425.
[11] M.J. Gorbunoff, Anal. Biochem. 136 (1984) 433.
[12] M.J. Gorbunoff, Anal. Biochem. 136 (1984) 440.
[13] T. Kawasaki, J. Chromatogr. 544 (1991) 147.
[14] P.K. Ng, J. He, P. Gagnon, J. Chromatogr. A 1142 (2007) 13.
[15] S. Schubert, R. Freitag, J. Chromatogr. A 1216 (2009) 3831.
[16] P. Gagnon, C.-W. Cheung, P.J. Yazaki, J. Sep. Sci. 32 (2009) 3857.
[17] CHT® Ceramic Hydroxyapatite–Instruction Manual, Bio-Rad Laboratories, 2009.
[18] A.N. Smith, A.M. Posner, J.P. Quirk, J. Colloid Interface Sci. 54 (1976) 176.
[19] J.C. Gramain, J.C. Voegel, M. Gumper, J.M. Thomann, J. Colloid Interface Sci. 118 (1987) 148.
[20] T.E. Gills, National Institute of Standards & Technology, Standard Reference Material 2910—Calcium Hydroxyapatite, Gaitherburg, MS, USA, 1997.
[21] C.W. Davies, Ion Association, Butterworths, London, 1962.
[22] L.J. Cummings, Paper Presented at SPICA 2008—Symposium on Preparative and Industrial Chromatography and Allied Techniques, Zurich, Switzerland, 2008.
[23] R.J. Beynon, J.S. Easterby, Buffer Solutions—The Basics, Oxford University Press, Oxford, UK, 1996.
[24] T.M. Pabst, G. Carta, J. Chromatogr. A 1142 (2007) 19.
[25] S. Ghose, T.M. McNerney, B. Hubbard, Biotechnol. Progr. 18 (2002) 530.
[26] J. Soto Pérez, D.D. Frey, Biotechnol. Progr. 21 (2005) 902.
[27] S.K. Doss, J. Dent. Res. 55 (1976) 1067.
[28] P. Gasser, J.C. Voegel, Ph. Gramain, Colloids Surf. A: Phys. Eng. Aspects 74 (1993) 275.
[29] I.S. Harding, N. Rashid, K.A. Hing, Biomaterials 26 (2005) 6818.
[30] H.C. Hodge, G. van Huysen, J.F. Bonner, S.N. van Voorhis, J. Biol. Chem. (1940) 451.
[31] S. Shimbayashi, H. Fukuda, T. Aoyama, M. Nakagaki, Chem. Pharm. Bull. 30 (1982) 3074.
[32] D. Fukegawa, S. Hayakawa, Y. Yoshida, K. Suzuki, A. Osaka, B. van Meerbeek, J. Dent. Res. 85 (2006) 941.
[33] F. Helfferich, Ion Exchange, McGraw-Hill, 1962.
[34] F. Helfferich, G. Klein, Multicomponent Chromatography: Theory of Interference, Marcel Dekker, Ann Arbor, MI, USA, 1970.